Estimation of the solute diffusion coefficient of a dilute liquid alloy: static structure factor and isothermal compressibility estimates obtained using the rational function approximation of the radial distribution

2009 J. Phys.: Condens. Matter 21 335104

(http://iopscience.iop.org/0953-8984/21/33/335104)

IOP PUBLISHING JOURNAL OF PHYSICS: CONDENSED MATTER

J. Phys.: Condens. Matter **21** (2009) 335104 (9pp) doi:10.1088/0953-8984/21/33/335104

Estimation of the solute diffusion coefficient of a dilute liquid alloy: static structure factor and isothermal compressibility estimates obtained using the rational function approximation of the radial distribution

Paul J Scott and Reginald W Smith

Department of Mechanical and Materials Engineering, Queen's University, Kingston, ON, K7L 3N6, Canada

E-mail: pjs7@queensu.ca

Received 11 March 2009, in final form 23 June 2009
Published 13 July 2009
Online at stacks.iop.org/JPhysCM/21/335104

Abstract

A simple method for estimating the mass diffusion coefficient of a dilute binary liquid alloy that sequentially uses experimental data for the static structure factor and isothermal susceptibility of the solvent is presented, as well as another using the static structure factor alone and a method using the isothermal susceptibility alone. A fourth method that simultaneously uses the static structure factor and isothermal susceptibility is also noted. Of significance is the fact that these methods do not require information about the interatomic potential. Stability with respect to weights in the optimization process employed has been established and is reported, as well as some indication of the upper limits on the applicable solute concentration. Comparisons are made with results from a high quality capillary experiment for Pb 1 wt% Au liquid alloy performed in microgravity, and with velocity autocorrelation estimates derived from molecular dynamics simulation. The results suggest that the capillary experiments are influenced by reverse diffusion of the solvent, and actually measure an average of the mass diffusion coefficients, D_{ij}, weighted by the equilibrium concentrations of the solvent, x_1, and solute, x_2, defined by

$$D_{\text{tot}} = x_1^2 D_{11} + x_2^2 D_{22}.$$

The three methods are required to provide upper and lower estimates for the mixed solvent–solute diffusion coefficient, which is not directly accessible from the experimental data, and demonstrate agreement with the experiment via D_{tot}.

1. Introduction

Our goal is to seek an independent theoretical verification of the high quality experimental estimates of the mass diffusion coefficient in a number of dilute molten metallic and metalloid alloys performed by Smith *et al* [1] on the Russian Space Station 'MIR' and the United States 'Shuttle'. In low-earth orbit, the gravitational forces are normally very small and so the usual long capillary diffusion couple experiment may be performed with a minimum of gravity-driven solute transport. Whilst in orbit, the residual atmospheric 'drag' on the space vehicle is small (approximately $5 \times 10^{-6} g$ where g is the terrestrial gravitational acceleration), however the transitory short period changes in g, referred to as 'g-jitter', caused by momentum changes within the space vehicle, may be significant e.g. at times these may have magnitude

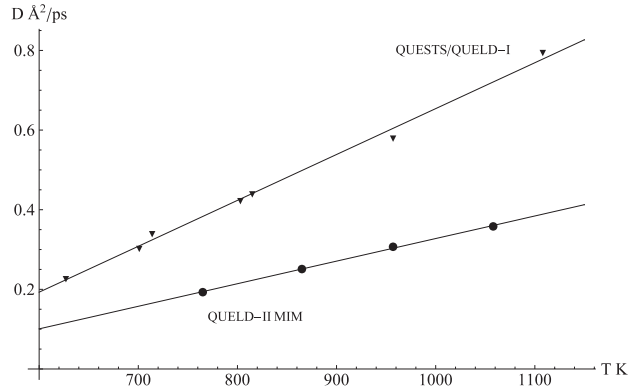

Figure 1. Pb 1 wt% Au diffusion coefficient versus temperature. QUESTS/QUELD-I without isolation mount, QUELD-II MIM with isolation showing the significant difference in diffusion coefficients with and without g-jitter. Both from Smith *et al* [1].

of $10^{-3}g$, and so cause significant solute transport and thus inflation of the value of any diffusion coefficient (D) being measured. The experimental work carried out on MIR was performed with the aid of the Canadian Space Agency microgravity isolation mount (MIM) to reduce the g-jitter experienced by the sample and produced values of 'D' lower than those obtained on the Shuttle for duplicate diffusion couples. Figure 1 shows the QUELD-I shuttle results and MIR based QUELD-II MIM results. Significant differences are evident and indicate different fluid regimes are in effect with and without g-jitter, and which are beyond the application of linear stability analysis or error analysis based on small perturbations to explain. In our earlier predictions, the value of 'D' for gold in a Pb 1 wt% Au alloy diffusion couple, Scott *et al* [2], molecular dynamics simulation was used along with velocity autocorrelation techniques to estimate the diffusion coefficient. The molecular dynamics results were also used to provide some of the terms required in the Enskog equation for the diffusion coefficients in the hard sphere liquid [3] to make comparisons. However, a prerequisite for realistic molecular dynamics predictions is the use of realistic values of the interatomic potentials for the alloy system being modelled. Unfortunately, good interatomic potentials are hard to find in the literature and enormously labour intensive to generate, often requiring detailed *ab initio* quantum mechanics calculation guided by a comprehensive set of experimental parameters [4, 5]. In view of this, alternative approaches to the problem of predicting values of 'D' for any given alloy system and temperature are presented here that do not require interatomic potentials.

Consider a nonreacting liquid free of external forces at a constant temperature T with number density ρ, which may vary in time t and place $\mathbf{r}$ where $\mathbf{r} \in D$ a closed bounded subset of $\mathbb{R}^3$, so $\rho = \rho(t, \mathbf{r})$, and having velocity $v(t, \mathbf{r})$. Let the liquid consist of N different species of atoms, denoted by i and j, having number concentrations $x_i(t, \mathbf{r})$. Assume in addition that momentum transport can be neglected. Then, the hydrodynamic equations describing the liquid in section 54 [6], reduce to conservation of mass and consist of the equation of continuity:

$$\partial_t \rho + \nabla \cdot \rho v = 0$$

and for each species i, $1 \leqslant i \leqslant N$ concentration equations:

$$\partial_t x_i + \nabla x_i \cdot v = -\nabla \cdot J_i = -\sum_{j=1}^{N} \nabla \cdot (D_{ij} \nabla x_j) \tag{1}$$

where D_{ij} are the mass diffusion coefficients, (mass diffusivities), which, by the Onsanger reciprocity [7], satisfies the symmetry $D_{ij} = D_{ji}$. In addition, to preserve total mass, the total mass flux must be zero, so the species flux J_i satisfy

$$\sum_{i=1}^{N} J_i = 0.$$

These mass diffusion coefficients are what is of interest here.

The basis of the estimates presented here is the Enskog equation for the interspecies mass diffusion coefficients D_{ij} [3]. Based on [8] a brief derivation of the Enskog equation follows. For now let the uniform liquid consist of N hard sphere species with species i having an atom diameter σ_i, atom mass m_i and number concentration x_i. The interspecies reduced mass is defined by $\mu_{ij} = m_i m_j/(m_i + m_j)$ and interspecies diameters be $\sigma_{ij} = (\sigma_i + \sigma_j)/2$. Let r denote the distance between the centres of hard sphere atoms of type i and j, the 'interatomic distance', then partial radial distribution functions [9] are denoted by $g_{ij}(r)$ and have the following pRDF property:

> Let Δ be a disk of circular cross section with area A and thickness dr and let an i-atom reside on the axis of the disk at a distance r from the disk. Then the expected number of j-atoms in the disk is $\rho g_{ij}(r) A dr$.

The Enskog equation may be obtained from the Einstein relation, derived from the Langevin equation for Brownian motion, that expresses interspecies mass diffusion coefficients as

$$D_{ij} = \frac{k_B T}{\zeta_{ij}} \tag{2}$$

with Boltzmann constant k_B and ζ_{ij} denoting the friction on an i-atom due to nearby j-atoms. ζ_{ij} is determined by the expected change in momentum due to j-atoms over a short time interval τ and is given by

$$\zeta_{ij} = \frac{\langle \Delta p \cdot \Delta p \rangle}{2 k_B T \tau}. \tag{3}$$

Although this may not be appropriate for dense fluids, assume there exist sufficiently small time intervals τ such that a j-atom collides only once with the i-atom during τ. Due to the conservation of linear momentum and kinetic energy, the change in i-atom momentum due to the collision is

$$\delta p_{ij} = 2\mu_{ij} \left(v_j - v_i\right) \cdot \left(\frac{r_j - r_i}{\|r_j - r_i\|} \right)$$

with r_i and r_j being the positions of the i-atom and j-atom at collision. The total change of momentum is given by the

sum of momentum changes over the j-atoms that reside in a collision volume that consists of a cylinder having length $\tau\|v_j - v_i\|$ and circular cross section with area $\pi\sigma_{ij}^2$, with the i-atom on the axis at the collision end. For τ sufficiently small, the pRDF property gives the expected number of j-atoms in the collision volume as the volume $\times\rho g_{ij}(\sigma_{ij})$. Summing over the expected j-atoms, the expected total change of momentum is

$$\begin{aligned}\langle\Delta p\cdot\Delta p\rangle &= 4\mu_{ij}^2\left(\left(v_j - v_i\right)\cdot\left(\frac{r_j - r_i}{\|r_j - r_i\|}\right)\right)^2\\ &\times \pi\sigma_{ij}^2\tau\|v_j - v_i\|\rho g_{ij}(\sigma_{ij}) = 4\mu_{ij}^2\|v_j - v_i\|^2\|r_{ij}\|^2\\ &\times \cos(\theta_{ij})^2\pi\sigma_{ij}^2\tau\|v_j - v_i\|\rho g_{ij}(\sigma_{ij}) \qquad (4)\end{aligned}$$

with θ_{ij} being the acute angle made by the unit vector $r_{ij} = (r_j - r_i)/\|r_j - r_i\|$ and the axis of the cylinder. The sum over j-atoms in the collision cylinder can be expressed by integrating the unit vector over its intersection with the collision cylinder, which requires that $0 \leqslant \theta \leqslant \pi/2$. Introducing an orthogonal basis $\{e_1, e_2, e_3\}$, with e_3 along the axis of the collision cylinder, and angle ψ extending around the circumference of the collision cylinder so that $-\pi \leqslant \psi \leqslant \pi$, the unit vector may then be expressed as $r_{ij} = \cos(\psi)\sin(\theta)e_1 + \sin(\psi)\sin(\theta)e_2 + \cos(\theta)e_3$ and so (4) becomes

$$\begin{aligned}\langle\Delta p\cdot\Delta p\rangle &= 4\pi\tau\rho\mu_{ij}^2\sigma_{ij}^2 g_{ij}(\sigma_{ij})\\ &\times\int_{-\pi}^{\pi}\int_0^{\frac{\pi}{2}}\|v_j - v_i\|^3(\cos(\psi)^2\sin(\theta)^2\\ &+ \sin(\psi)^2\sin(\theta)^2 + \cos(\theta)^2)\cos(\theta)^2\,\mathrm{d}\theta\,\mathrm{d}\psi. \qquad (5)\end{aligned}$$

To complete the expression it is necessary to take the expectation over the atom velocities v_i and v_j using the equilibrium probability density, and remembering that although there is no restriction on v_i, for each v_i, v_j is restricted so a collision is possible. Substitution of the completed form of (5) and substitution of (3) into (2) results in the Enskog equation for the mass diffusion coefficients:

$$D_{ij} = \frac{3}{8\rho g_{ij}(\sigma_{ij})\sigma_{ij}^2}\left(\frac{k_\mathrm{B}T}{2\pi\mu_{ij}}\right)^{\frac{1}{2}}. \qquad (6)$$

Most of the variables in (6) are obvious, with the species radii, σ_i, being the unknown, that must be determined. The hard sphere partial radial distribution functions, $g_{ij}(r)$ must also be approximated.

However other equations for the diffusion coefficients are possible. In terms of the velocity correlation with respect to the equilibrium distribution the Green–Kubo equation for the mass diffusion coefficient of a single species liquid is

$$D = \tfrac{1}{3}\int_0^\infty\langle v(t)\cdot v(0)\rangle\,\mathrm{d}t. \qquad (7)$$

When the coupled diffusion system is viewed as diffusion within one mixed liquid, a total mass diffusion coefficient, D_{tot}, is defined by

$$\begin{aligned}D_{\mathrm{tot}} &= \frac{1}{3}\int_0^\infty\left\langle\left(\sum_{i=1}^N x_i v_i(t)\cdot\sum_{j=1}^N x_j v_j(0)\right)\right\rangle\mathrm{d}t\\ &= \sum_{i=1}^N x_i^2 D_{ii} \qquad (8)\end{aligned}$$

where for dilute alloys with x_i is small for $2 \leqslant i \leqslant N$

$$D_{\mathrm{tot}} \approx D_{11}.$$

In the following evaluation of (6) is required, and to do so the hard sphere partial radial distribution functions, $g_{ij}(r)$ must be approximated. The Percus–Yevick approximation of $g_{ij}(r)$ [10], is fairly easy to implement, however it is not thermodynamically consistent. More recently the rational function approximation for the partial radial distribution functions, presented in [11, 12], and which is thermodynamically consistent, has proved to be effective. Following [13], a brief introduction to the rational function approximation is given.

For $n = 1, 2, 3$ let

$$\xi_n = \rho\sum_{i=1}^N x_i\sigma_i^n \qquad (9)$$

and define the volume packing fraction by

$$\eta = \frac{\pi}{6}\xi_3. \qquad (10)$$

The partial radial distribution function at the interspecies diameters are given by the GHLL expression, see [13],

$$g_{ij}(\sigma_{ij}) = \frac{1}{2\pi}\left(\lambda + \frac{1}{2}\lambda'\frac{\sigma_i\sigma_j}{\sigma_{ij}} + \frac{1}{18}\frac{\lambda'^2}{\lambda}\frac{\sigma_i^2\sigma_j^2}{\sigma_{ij}^2}\right) \qquad (11)$$

with $\lambda = 2\pi/(1-\eta)$ and $\lambda' = \pi^2\xi_2/(1-\eta)^2$. For a multispecies hard sphere fluid, the equation of state is given by

$$p = \rho k_\mathrm{B}T\left(1 + \frac{2}{3}\pi\rho\Sigma_{i=1}^N\Sigma_{j=1}^N x_i x_j\sigma_{ij}^3 g_{ij}(\sigma_{ij})\right)$$

with p denoting pressure and k_B Boltzmann's constant. Substitution of (11) into this equation gives the BMCSL, see [13], equation of state [13]. The isothermal susceptibility χ satisfies

$$\frac{1}{\chi} = \frac{1}{k_\mathrm{B}T}\left(\frac{\partial p}{\partial\rho}\right)_T.$$

Substitution of the BMCSL into this equation gives the following equation for the isothermal susceptibility

$$\chi = \frac{\rho}{\frac{\rho}{(1-\eta)^2} + \pi\frac{\zeta_1\zeta_2}{(1-\eta)^3} + \frac{\pi^2}{36}\zeta_2^3\frac{9-4\eta+\eta^2}{(1-\eta)^4}}. \qquad (12)$$

As long as (11) and (12) are used in the following development, the hard sphere fluid is thermodynamically consistent.

Now let $G_{ij}(s)$ be defined by the Laplace transform

$$G_{ij}(s) = \int_0^\infty \mathrm{e}^{-sr}g_{ij}(r)r\,\mathrm{d}r$$

so g_{ij} is obtained from an inverse Laplace transform of G_{ij}, and a computational form is sought for G_{ij}. From the bounded properties of g_{ij} and isothermal susceptibility, it can be shown

Table 1. Input variables for Mathematica programs to evaluate the rational function approximation of the partial radial distribution function.

Mathematica variable	Meaning	Remark
nco	number of species N_s	
ratio	$\{1, \sigma_2/\sigma_1, \ldots, \sigma_{\mathrm{nco}}/\sigma_1\}$	Vector of nondimensional atom diameters
con	$\{x_1, \ldots, x_{\mathrm{nco}}\}$	Vector of species number concentrations
eeta	$\frac{\pi}{6}\rho\sigma_1^3 \sum_{i=1}^{\mathrm{nco}} x_i(\frac{\sigma_i}{\sigma_1})^3$	Nondimensional packing fraction η^*

that G_{ij} has the form

$$G_{ij}(s) = \frac{\mathrm{e}^{-s\sigma_{ij}}}{2\pi s^2}\left[L(s)\cdot[(1+\alpha s)\mathbb{1} - A(s)]^{-1}\right]_{ij}$$

with the $N \times N$ identity matrix $\mathbb{1}$ and an, as yet unknown, positive parameter α. The components of matrix $L(s)$ are expressed as

$$L_{ij}(s) = L^0_{ij} + L^1_{ij}s + L^2_{ij}s^2$$

and matrix $A(s)$ is expressed as

$$A(s) = \sum_{n=0}^{\infty} A^n s^n \tag{13}$$

with the components of matrix A^n expressed in terms of the components of $L(s)$ as

$$A^n_{ij} = (-1)^n \rho x_i \times \left(\frac{\sigma_i^{n+3}}{(n+3)!}L^0_{ij} - \frac{\sigma_i^{n+2}}{(n+2)!}L^1_{ij} + \frac{\sigma_i^{n+1}}{(n+1)!}L^2_{ij}\right)$$

and

$$L^0_{ij} = \lambda + \lambda'\sigma_i + 2\lambda'\alpha - \lambda\rho\sum_{k=1}^{N} x_k\sigma_k L^2_{kj}$$

$$L^1_{ij} = \lambda\sigma_{ij} + \tfrac{1}{2}\lambda'\sigma_i\sigma_j + (\lambda + \lambda'\sigma_i)\alpha - \tfrac{1}{2}\lambda\rho\sigma_i\sum_{k=1}^{N} x_k\sigma_k L^2_{kj}$$

$$L^2_{ij} = 2\pi\sigma_{ij}g_{ij}(\sigma_{ij})\alpha. \tag{14}$$

After determining a suitable finite upper limit in (13), and the substitution of (11) in (14), this becomes a complete specification of $G_{ij}(s)$ when α is given. To find α, the Ornstein–Zernike equation [9], is used to express the isothermal susceptibility as

$$\frac{1}{\chi} = \sum_{i=1}^{\infty}\sum_{j=1}^{\infty}\sqrt{x_i x_j}\left[\mathbb{1} + \hat{h}(0)\right]^{-1}_{ij} \tag{15}$$

with the components of $\hat{h}(0)$ given by

$$\hat{h}_{ij}(0) = -4\pi\rho\sqrt{x_i x_j}\left[B^1\cdot\left[\mathbb{1} - A^0\right]^{-1}\right]_{ij} \tag{16}$$

and the components of B^1 are given by

$$B^1_{ij} = \sum_{k=1}^{N} A^3_{kj} + \sum_{k=1}^{N}\sigma_{ik}A^2_{kj} - \sum_{k=1}^{N}(\tfrac{1}{2}\sigma^2_{ik} + H^0_{ik})(\alpha\delta_{kj} - A^1_{kj}) - \sum_{k=1}^{N}(\tfrac{1}{6}\sigma^3_{ik} + \sigma_{ik}H^0_{ik})(\delta_{kj} - A^0_{kj}) \tag{17}$$

$$H^0_{ij} = [B^0\cdot[\mathbb{1} - A^0]^{-1}]_{ij} \tag{18}$$

$$B^0_{ij} = \sigma_{ij}g_{ij}(\sigma_{ij})\alpha + \sum_{k=1}^{N}A^2_{kj} - \sum_{k=1}^{N}\sigma_{ik}(\alpha\delta_{kj} - A^1_{kj}) - \sum_{k=1}^{N}\tfrac{1}{2}\sigma^2_{ik}(\delta_{kj} - A^0_{kj}). \tag{19}$$

Substitution of (11) and (12) in (15) and the use of (16)–(19), results in an equation for α. This equation for α is a ratio of two polynomials of degree $2N$, and hence is a rational function approximation. For physical reasons the smallest real root is chosen. When both α and the matrix L^0 are set to zero the above procedure reduces to the Percus–Yevick approximation [10].

Since parts of the calculation involve symbolic algebra, and are not purely numerical, the present code for the partial radial distribution functions is only available in Mathematica [14]. To use these programs, the variables listed in table 1 must be used. To demonstrate their results, Yuste *et al* [13], nondimensionalized the interatomic distance r by dividing by the diameter of the first species, σ_1, usually chosen to be the largest diameter. To maintain consistency and enable comparison with these results, the same nondimensionalization was used here, hence the definition of ratio in table 1. If the physical density is ρ, the nondimensional density becomes $\rho\sigma_1^3$. In many studies of abstract hard sphere fluids, the volume fraction η is used as an invariant parameter. Here, the value of η for a specific alloy, Pb 1 wt% Au, must be preserved, hence the definition of η^*.

Mathematica [15], has also been used here for all additional calculations.

2. Estimation of hard sphere equivalent atomic diameters

Experimental data about the density of liquid lead is available in [16]. From this a linear relation for the number density, N Å^{-3} of the Pb 1 wt% Au liquid alloy in terms of temperature T K was devised:

$$\rho(T) = 0.032\,347 - 0.4069\times10^{-5}(T - 273). \tag{20}$$

For a one species liquid, the static structure factor is obtained from the radial distribution function by a Fourier sine transform:

$$S_{11}(q) = 1 + 4\pi\rho\int_0^{\infty}(g_{11}(r) - 1)\,\frac{\sin(qr)}{q}r\,\mathrm{d}r \tag{21}$$

where q has units Å^{-1}. Since $g_{11}(r) \to 1$ fairly quickly as r increases, a finite integral with upper limit 30 Å is

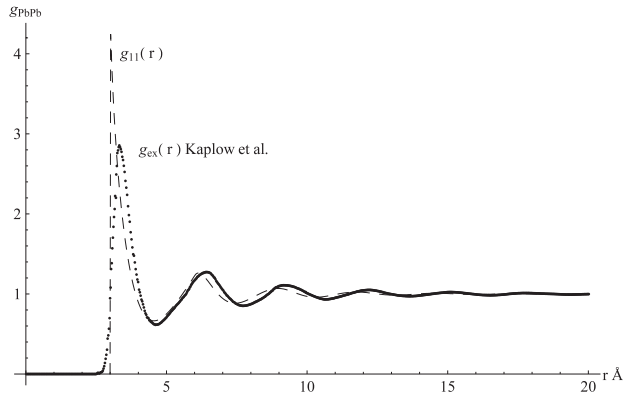

Figure 2. For $T = 602$ K g_{ex} Kaplow *et al* [17] and optimal g_{11} for Pb solvent versus interatomic distance r Å. The optimal fits at higher temperatures are similar. Since, for hard sphere liquid g_{11} has a sharp peak at the atom diameter, it always tends to overshoot the rounded first peak of the experimental data. However the distribution of neighbouring atoms, given by the dampened waveform, is in good agreement with g_{ex}.

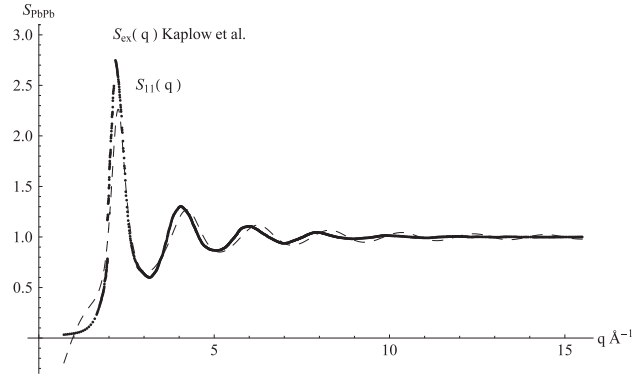

Figure 3. For $T = 602$ K S_{ex} Kaplow *et al* [17] and optimal S_{11} for Pb solvent. The optimal fits at higher temperatures are similar.

usually sufficient. The static structure factor can be measured experimentally by neutron scattering [9], during which the scattering intensity [17] determines q. For Pb, is available at temperatures over the liquid temperature range. For the following temperatures, experimental values of the static structure factor, $S_{ex}(q)$ and the radial distribution function, $g_{ex}(r)$, are available for pure Pb: 602 K in [17], 613 K in [18], 623 K in [19], 643 K in [20], 660 K in [21], 723 K in [19], 823 K in [19], 863 K in [20], 873 K in [18], 1053 K in [18], and 1163 K in [20].

Values for the isothermal compressibility of liquid lead are found in [22] and [23]. From this the following expression for the isothermal susceptibility as a linear function of the temperature can be derived:

$$\chi_{ex}(T) = -0.011\,043\,395 + 0.323\,0992 \times 10^{-4} T.$$

At any temperature, for a binary alloy (12), depends on the two hard sphere diameters σ_1 and σ_2, and the isothermal susceptibility is expressed as $\chi(\rho(T), \sigma_1, \sigma_2)$. Then

$$\chi_{ex}(T) = \chi(\rho(T), \sigma_1, \sigma_2) \tag{22}$$

gives a relation for σ_1 and σ_2.

3. Methods for mass diffusion coefficient estimation

A two step method for estimating σ_1 and σ_2 by using the static structure factor and isothermal compressibility now follows.

Step one for a dilute alloy, one assumes g_{11} and S_{11} of the solvent in the alloy are the same as g_{ex} and S_{ex} of the pure solvent. For given experimental data, one may find the hard sphere equivalent atomic diameter of the solvent, σ_1, by minimizing the functional

$$M(\sigma_1) = \left(w_{RDF} \int_0^\infty (g_{ex}(r) - g_{11}(r))^2 \, dr + w_{SSF} \int_0^\infty (S_{ex}(q) - S_{11}(q))^2 \, dq \right)^{\frac{1}{2}} \tag{23}$$

Table 2. Optimal σ_1 over convex weights $w_{RDF} + w_{SSF} = 1$ showing only a small change in σ_1 with different weights.

w_{RDF}	w_{SSF}	σ_1 (Å)
0.1	0.9	3.032 38
0.2	0.8	3.000 23
0.3	0.7	3.000 05
0.4	0.6	3.000 03
0.5	0.5	3.000 02
0.6	0.4	3.000 02
0.7	0.3	3.000 02
0.8	0.2	2.993 92
0.9	0.1	2.993 92

with g_{11} given by the rational function approximation. With regard to table 1, the inputs are nco = 1, ratio = {1}, con = {1}, and eeta = $\frac{\pi}{6}\rho\sigma_1^3$, with σ_1 being the candidate value for the solvent atom hard sphere diameter. S_{11} is given by Fourier sine transform (21). As indicated previously, finite upper limits are sufficient for both integrals. In theory, g_{ij} and S_{ij} are uniquely related via the Fourier transform so it should be sufficient to either optimally fit g_{11} or S_{11}. However, the resolution of S_{ex} and g_{ex} varied, in some cases consisting of tables of values to a small number of decimal places, and sometimes requiring digitizing graphs, which in itself introduces some mechanical and subjective errors. Also, oscillating residual error often occurred in g_{ex} at small radii, and negative values of S_{ex} occurred at small values of q. The user of these data is required to reach a subjective judgement about how to deal with these effects. The above simultaneous optimization was chosen to reduce effects occurring independently in g_{ex} and or S_{ex}. The weights w_{RDF} and w_{SSF} were added to determine how changes in the relative importance of the two terms in the cost function changes the optimal value of σ_1. Table 2 shows the values of optimal σ_1 over a convex combination of weights.

The optimal σ_1 changes only slightly with different weights, so the procedure is stable. In the following equal weights were chosen so $w_{RDF} = w_{SSF} = 1$. For $T = 602$ K, the resulting solution with equal weights is exhibited in figures 2 and 3.

From figure 2 it is clear that the optimal value of the solvent hard sphere diameter is approximately $\sigma_1 = 3.032\,24$ Å.

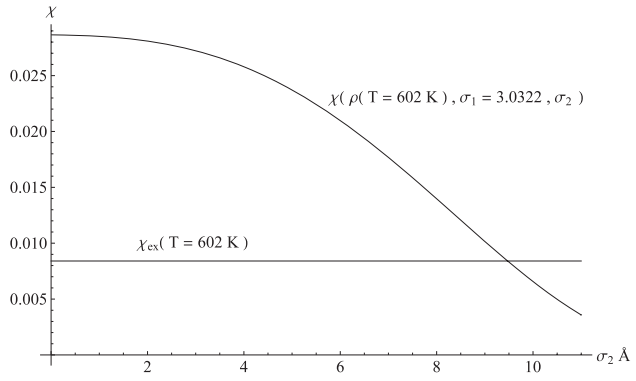

Figure 4. Using the solvent diameter found in step one, the intersection of the experimental isothermal susceptibility value $\chi_{ex}(T = 602\ \text{K})$ with the computed isothermal susceptibility $\chi(\rho(T = 602\ \text{K}), \sigma_1 = 3.0322, \sigma_2)$ determines the solvent diameter $\sigma_2 \approx 9.5$ Å.

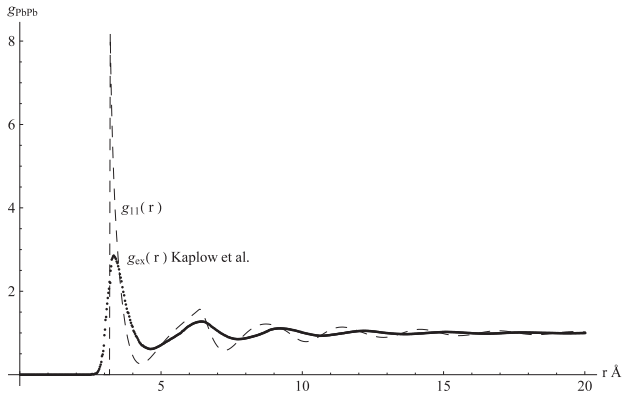

Figure 5. Method D at $T = 602$ K g_{ex} Kaplow *et al* [17] and optimal g_{11} for Pb solvent versus interatomic distance r Å. Clearly not as good as method 1 shown in figure 2.

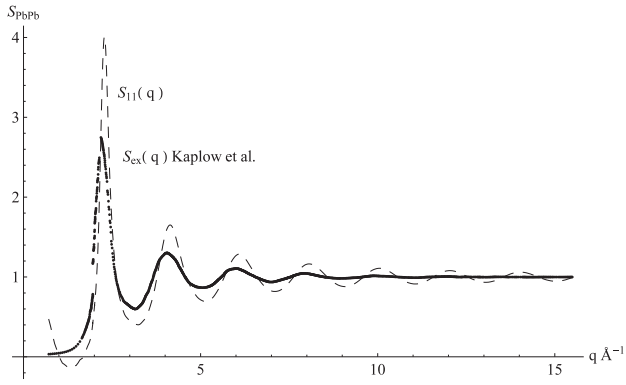

Figure 6. Method D static structure factor comparison. Clearly not as good as method 1 shown in figure 3.

With σ_1 given by step one (22), is a relation for σ_2. Step two consists of solving this relation subject to the constraints that σ_2 must remain real and positive. Figure 4 exhibits this step for $T = 602$ K. The numerical solution is $\sigma_2 = 9.474$ Å.

Substituting $\sigma_1 = 3.032\,24$ Å and $\sigma_2 = 9.474$ Å gives $g_{12}(\sigma_{12}) = 13.4041$, with $\eta = 0.5931$ and substitution into (6) gives at $T = 602$ K the solute mass diffusion coefficient $D_{12} = 0.0205$ Å^2 ps^{-1}. Method A has been carried out at each of the temperatures listed above. The results are exhibited in table 3.

The radial distribution function nearest peak distance for liquid Pb near the melting temperature, listed in table II of Protopapas *et al* [24], is $d_{Pb} = 3.39$ Å. This suggests the values of σ_1 listed in table 3, found in step one, are underestimations. The large values of σ_2 in the table, may result from satisfying the isothermal susceptibility relation (22), while compensating for a consistent error in the values of σ_1 supplied by step one. This may be further amplified since the solute concentration is low and the compensating effect is achieved through a comparatively small number of atoms.

To develop additional methods assume the concentration of the solute is sufficiently low that the size of the solute atoms has no role. Consequently both types of atoms have the same effective hard sphere diameter. In method B the equal radii are substituted into (22) and (23) is not required. In method C the equal radii are substituted into (23), and (22) is not required. Notice that, with equal radii, $g_{ij}(\sigma_{ij})$ given by (11) are the same, so with solvent Pb and solute Au having almost identical atomic weight, the diffusion coefficients D_{ij} given by (6) are almost identical. So, for each of methods B and C, only one diffusion coefficient is considered: $D^B \equiv D^B_{12}$ and $D^C \equiv D^C_{12}$.

A fourth method, method D, consists of simultaneously solving (23) and (22). Briefly, for a candidate value of σ_1 a value of σ_2 is found by solving (22) and (23) is evaluated with g_{11} given by inputs: nco $= 2$, ratio $= \{1, \sigma_2/\sigma_1\}$, con $= \{x_1, x_2\}$, and eeta $= \frac{\pi}{6}\rho\sigma_1^3(x_1 + x_2(\sigma_2/\sigma_1)^3)$. At $T = 602$ K the resulting optimal values of σ_1 and σ_1 give the comparisons with experimental data shown in figures 5 and 6. Method D does not satisfy the minimization of (23) as well as method A, and is not considered further. The methods are summarized in table 4.

4. Results for Pb 1 wt% Au liquid

All three methods were applied to the Pb 1 wt% Au alloy over its liquid temperature range. Molecular dynamic simulations of single species hard sphere liquids indicate that starting at volume fraction $\eta = 0.56$ a transition into a glassy solid begins, which is complete at $\eta = 0.64$ [13]. Figure 7 shows the packing fraction remains within the hard sphere liquid range $\eta \leqslant 5.6$ throughout most of the temperature range for all three methods. Since the solvent and solute radii are equal in method B, the transition criteria should apply, and indicates transitional behaviour for $T \leqslant 625$ K, which is consistent with the melting temperature of Pb 1 wt% Au, $T_m \approx 598$ K. The large solute diameter given by method A results in high values of η. However, this also means the transition criteria is less appropriate, and the upper transition limit, $T = 720$ K, is an over estimate. Figure 8 shows that methods B and C give almost the same effective hard sphere diameters, although methods A and B give almost the same packing fraction. Figure 9 shows that the partial radial distribution function of method B is approximately mid-way between those of the other two methods.

Since the values of η in figure 7 suggest method B should give results similar to method A, the distinction between the

Table 3. Results for method A at temperatures were S_{ex} is available.

T (K)	σ_1 (Å)	σ_2 (Å)	ηN	$g_{12}(\sigma_{12})$	D_{11}^{A}	D_{12}^{A}	D_{22}^{A} (Å^2 ps^{-1})
602	3.0322	9.474	0.5931	13.4041	0.1334	0.0205	0.0035
613	3.0699	8.914	0.5849	12.9148	0.1338	0.0234	0.0045
623	3.0326	9.326	0.5849	12.7198	0.1420	0.0225	0.0040
643	3.0570	8.873	0.5751	12.0679	0.1473	0.0260	0.0051
660	3.0368	9.031	0.5713	11.6916	0.1567	0.0266	0.0050
723	3.0378	8.636	0.5514	10.3451	0.1824	0.0339	0.0070
823	3.0393	8.059	0.5247	8.8192	0.2234	0.0476	0.0113
863	3.0052	8.408	0.5191	8.4678	0.2467	0.0482	0.0106
873	3.0079	8.322	0.5165	8.3527	0.2504	0.0500	0.0112
1053	2.9880	7.943	0.4837	6.9244	0.3340	0.0729	0.0180
1163	2.9760	7.800	0.4673	6.3269	0.3877	0.0877	0.0225

Table 4. Summary of the methods.

Name		Step one	Step two	Diffusion coefficients
A	$\sigma_1 \neq \sigma_2$	σ_1 minimizes (23)	σ_2 satisfies (22) given σ_1	D_{11}^{A}, D_{12}^{A}, D_{22}^{A}, D_{tot}^{A}
B	$\sigma_1 = \sigma_2$	Satisfy (22)		D^{B}
C	$\sigma_1 = \sigma_2$	Minimize (23)		D^{C}
D	$\sigma_1 \neq \sigma_2$	Minimize (23) with (22)		

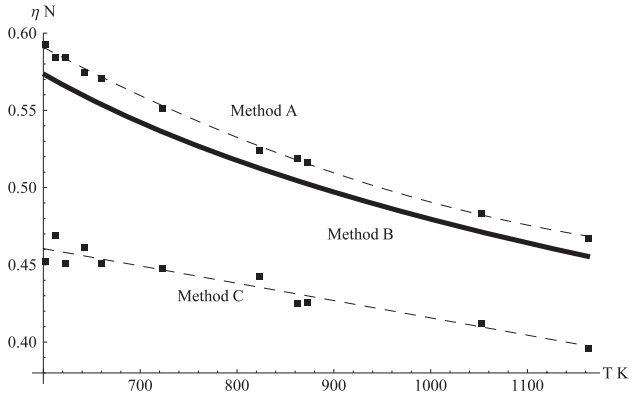

Figure 7. Packing fraction η of the three methods versus temperature. For method A and C there are results only at temperatures for which g_{ex} and S_{ex} are available, hence the square marker points. Method A and C markers have been connected with a linear or quadratic least squares fit, whichever was most appropriate, indicated by dashed lines. Since the experimental isothermal susceptibility is available at all temperatures, method B was applied using a temperature increment of $\Delta T = 10$ K, and the result is depicted with a solid curve without markers. Although the diameter of the Au hard sphere solute atoms for method A is much larger than for method B, the packing fractions are almost the same. When equal diameters are assumed in method C, the optimal fitting to g_{ex} and S_{ex} results in a smaller packing fraction than method A.

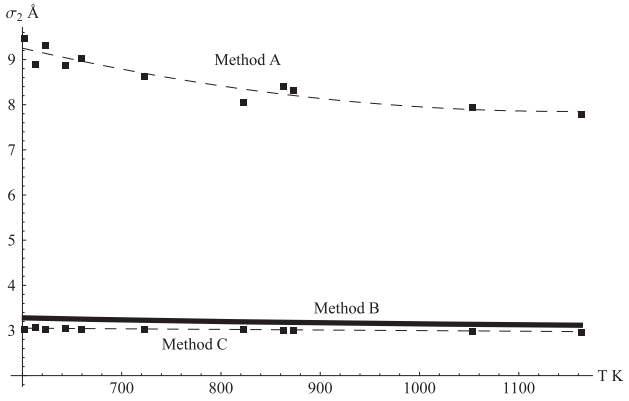

Figure 8. Solvent hard sphere radius σ_2 of the three methods versus temperature. Here method A and B differ significantly. The close agreement of method B and C indicate that for hard sphere models the isothermal susceptibility provides almost as much information as the entire static structure factor.

three methods brought out by the partial radial distribution function in figure 9 is central in the success of method B, and indicates the importance of an accurate estimate of the partial radial distribution function.

Before discussing the mass diffusion coefficients, recall the experimental results were obtained from capillary devices in which solute diffuses from an alloy plug into a column of pure solvent. A proportional schematic of the Pb 1 wt% Au capillary system is shown in figure 10.

Although the solute concentration is low in the alloy plug, there is still some reverse diffusion of solvent into the plug. This phenomenon was observed experimentally during solid diffusion by Kirkaldy [25] who noted movement of the interface between the plug and solvent, and in the analysis of the final concentration profile, introduced the final interface location as an additional variable to be determined as part of the estimation of the diffusion coefficient. D_{tot} defined by (8) is required to examine the results for the Pb 1 wt% Au capillary experiment.

Figure 11 shows the mass diffusion coefficient computed for each method compared with the experimental results in Smith *et al* [1] and the results from molecular dynamic MD simulation in Scott *et al* [2]. Note that D_{11}^{A}, D_{tot}^{A}, and D^{B} are in good agreement with the experimental results, which is consistent with the derivation of (8) and accompanying discussion. The close agreement of D^{C} with the MD estimates suggests this is an estimate of the mixed solvent–solute diffusion coefficient D_{12}. D_{12}^{A} and D_{22}^{A} are quite low because

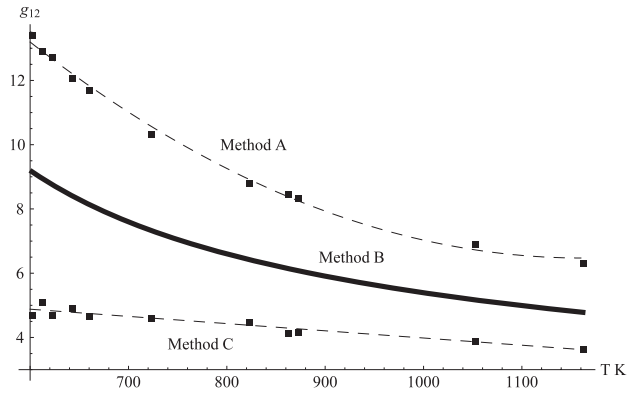

Figure 9. $g_{12}(\sigma_{12})$ of the three methods versus temperature. Method B identifies a balance between methods A and C which indicates the importance of the rational function approximation.

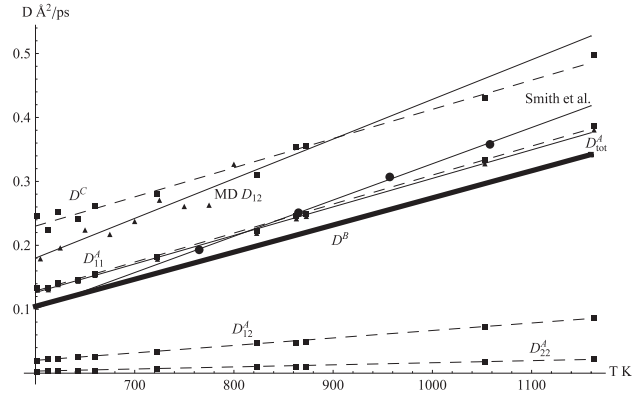

Figure 11. Diffusion coefficients of the three methods versus temperature compared with QUELD-II MIM experimental results from Smith *et al* [1] and estimates from molecular dynamic MD simulation from Scott *et al* [2]. The close agreement of D^{A}_{11}, $D^{\mathrm{A}}_{\mathrm{tot}}$, and D^{B} with the experimental results suggests the experiment is influenced by reverse solvent diffusion and the capillary experiment actually measures D_{tot}. Note the close agreement of D^{C} with the MD estimates. D^{A}_{12} and D^{A}_{22} are quite low because of the large solute diameter, σ_2, found by method A.

of the large solute diameter, σ_2, found by method A, however these serve as lower estimates.

Since only D_{tot} is directly measurable from the capillary experiment, while the other diffusion coefficients are inaccessible, it is clear that all three methods are required. In general, for capillary experiments in liquids, models for the individual diffusion coefficients must be provided, and the success of such models is determined by how well they estimate D_{tot}.

A large number of microgravity binary alloy diffusion experiments were performed with a 1 wt% solute concentration. However some consideration of the effect of concentration in the model results is desirable. First, for method B with $\sigma_1 = \sigma_2$ and $x_1 + x_2 = 1$, equations (9) and (10) remain constant regardless of changes in concentration, so (12) is constant and the solution of (22) for the radii is constant. Consequently, the value of $g_{12}(\sigma_{12})$ given by (11), is constant and the value of the diffusion coefficient given by (6) remains constant. Method B indicates no change in the diffusion coefficient as the concentrations change subject to $x_1 + x_2 = 1$. Since method C makes a one species evaluation of g_{11} with con $= \{1\}$ it cannot indicate changes as the concentrations change. Since method D simultaneously varies both radii it might indicate variations due to changes of concentration, although at low concentrations it does not perform as well as method 1. Method 1 was used at $T = 602$ K with the solute number concentration, $x_2 = x_{\mathrm{Au}}$ in the range $0.01 \leqslant x_{\mathrm{Au}} \leqslant 0.09$ The results became physically meaningless for $x_{\mathrm{Au}} > 0.06$, but below this limit they are shown in figures 12 and 13. Both figures exhibit linear rates of change in hard sphere radii and partial diffusion coefficients up to $x_{\mathrm{Au}} \approx 0.02$, as are to be expected with small differences in x_{Au}. However, above that value, inconsistent changes occur. Hence method A is limited to low solute number concentrations, i.e. less than 0.02. This also suggests that, even at fairly low solute number concentrations, information about the alloy isothermal compressibility and static structure factor, as well as, a simultaneous method such as method D, may be required to estimate how the mass diffusion coefficients vary with number concentration.

5. Conclusions

Three methods of obtaining estimates for the mass diffusion coefficient in dilute binary liquid alloys based on the rational function approximation of the partial radial distribution functions of the alloy, in [11, 12], have been described. One method sequentially uses static structure factor data and data about the isothermal compressibility of the solvent. The other two methods use either the static structure factor or the isothermal compressibility independently. A fourth method, method D, that simultaneously uses both the static structure factor and isothermal compressibility has also been discussed briefly. The stability of the first method with respect to variable weights in its optimization procedure has been demonstrated. It has been shown that two of the methods give no information about how mass diffusion coefficients vary

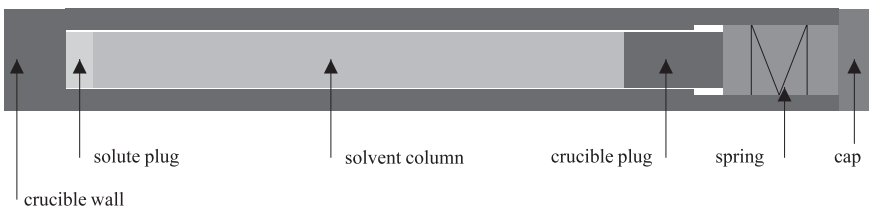

Figure 10. Proportional schematic of Pb 1 wt% Au capillary system.

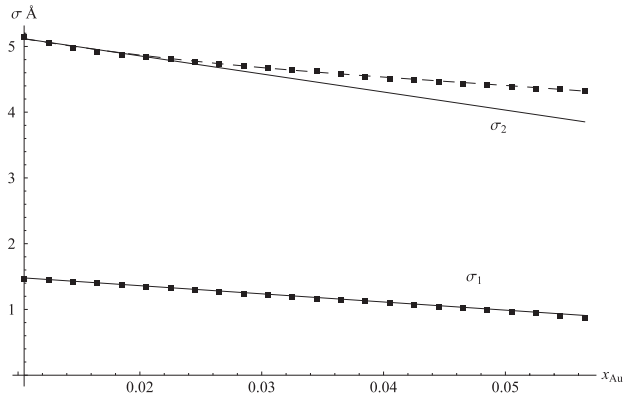

Figure 12. For method A hard sphere radii σ_1 and σ_2 versus solute number concentration $x_2 = x_{\mathrm{Au}}$. As x_{Au} increases a linear change in σ_2 is observed up to $x_{\mathrm{Au}} \approx .02$. The lower rate of decrease of σ_2 for $x_{\mathrm{Au}} > .02$ while σ_1 continues to decrease at the same rate suggests the onset of some numerical inconsistency.

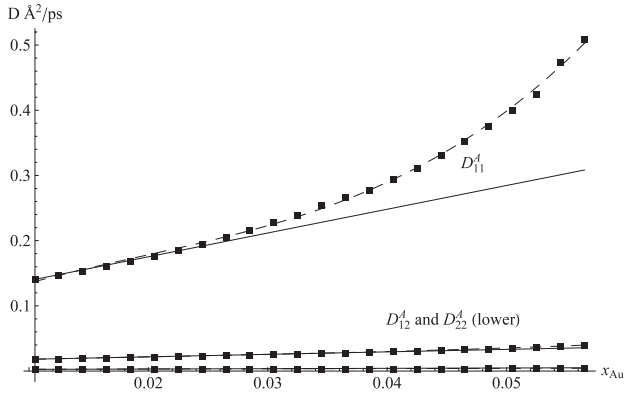

Figure 13. For method A the partial diffusion coefficients D_{11}^{A}, D_{12}^{A} and D_{22}^{A} versus solute number concentration $x_2 = x_{\mathrm{Au}}$. As x_{Au} increases a linear change in D_{11}^{A} is observed up to $x_{\mathrm{Au}} \approx .02$. The large rate of increase of D_{11}^{A} for $x_{\mathrm{Au}} > .02$ while D_{12}^{A} and D_{22}^{A} continue to increase at the same rates suggests the onset of some numerical inconsistency.

with solute concentration, while the first method appears to be reliable only at solute atom number concentrations below 0.02 wt%.

A total mass diffusion coefficient, D_{tot}, based on weighing the solvent and solute velocity fields by their equilibrium atom number concentrations has been introduced in order to discuss the results of capillary type diffusion experiments.

The methods have been applied to Pb 1 wt% Au liquid alloy and compared with high quality microgravity capillary experiment results using the Canadian Space Agency Microgravity Isolation Mount, Smith *et al* [1], and velocity autocorrelation estimates based on molecular dynamic MD simulation, Scott *et al* [2]. Via the total mass diffusion coefficient, D_{tot}, the three methods compare well with the experimental results. Comparison with the MD results suggests one of the methods gives a good estimate of the mixed solvent–solute diffusion coefficient, D_{12}. Lower estimates are also provided.

The results suggest that in general, since only the total diffusion coefficient, D_{tot}, is directly available from capillary experiments, several theoretical methods to estimate the other diffusion coefficients, and assessed on their ability to reproduce D_{tot} are required. When static structure factor data and data about the isothermal compressibility are available, these methods can be applied to other microgravity experimental results.

References

[1] Smith R W, Zhu X, Tunnicliffe M C, Smith T J N, Misener L and Adamson J 2002 *Ann. New York Acad. Sci.* **57** 974

[2] Scott P J and Smith R W 2008 *J. Appl. Phys.* **104** 043706

[3] Chapman S and Cowling T G 1929 *The Mathematical Theory of Nonuniform Gases* (London: Cambridge University Press)

[4] Mishin Y and Farkus D 1999 *Phys. Rev.* B **59** 3393–407

[5] Mishin Y, Mehi M J and Papaconstantopoulos D A 2002 *Phys. Rev.* B **65** 224114

[6] Woods L C 1986 *The Thermodynamics of Fluid Systems* (Oxford: Clarendon)

[7] Kreuzer H J 1981 *Nonequalibrium Thermodynamics and its Statistical Foundations* (Oxford: Clarendon)

[8] Helfund E 1961 *Phys. Fluids* **4** 681–91

[9] Hansen J P and McDonald I R 2006 *Theory of Simple Liquids* (Boston: Academic)

[10] Percus J K and Yevick G J 1958 *Phys. Rev.* **110** 1–13

[11] Yuste S B and Santos A 1991 *Phys. Rev.* A **43** 5418–23

[12] Yuste S B, de Haro M L and Santos A 1996 *Phys. Rev.* E **53** 4320–6

[13] Yuste S B, Santos A and de Haro M L 1998 *J. Chem. Phys.* **108** 3683–93

[14] http://www.unex.es/fisteor/santos/sby.html

[15] Wolfram Research Inc. 2008 *Mathematica Version 6.0.3, Champagne, Il*

[16] Schwaneke A E and Falke W L 1972 *J. Chem. Eng. Data* **17** 291–3

[17] Kaplow R, Strong S L and Averbach B L 1965 *Phys. Rev.* A **138** 1336–45

[18] North D M, Enderby J E and Egelstaff P A 1968 *J. Phys. C: Solid State Phys.* **1** 1075–87

[19] Steffen B 1976 *Phys. Rev.* B **13** 3227–31

[20] Dahlborg U, Davidovic M and Larsson K E 1977 *Phys. Chem. Liq.* **6** 149–66

[21] Blagoveshchenskii N M, Morozov V A, Novikov A G, Savostin V V, Shimkevich A L and Shimkevich I Y 2005 *Physica* B **364** 255–62

[22] Stojić M, Stojić B B and Milivojević D 2003 *Physica* B **334** 274–86

[23] Filippov S I, Kazakov N B and Pronin L A 1966 *Izv. Vuzov. Chem. Met.* **3** S8

[24] Protopapas P, Andersen H C and Parlee N A D 1973 *J. Chem. Phys.* **59** 15–25

[25] Kirkaldy J S and Young D J 1987 *Diffusion in the Condensed State* (London: The Institute of Metals)